Investigating Visual Neural Distinctiveness through fMRI and EEG modalities using Support Vector Machine Classification

Erin Knape

Department of Psychology, University of Michigan

Author Note

My deepest gratitude goes to Noah Reardon for his advice, staunch work ethic, and unwavering encouragement. Special thanks to my thesis predecessors, Ethan Nelson and Ryan Rich, who paved the way. Lastly, an enormous thanks goes to Dr. Molly Simmonite, Dr. Thad Polk, and the Polk Lab for this opportunity. I am immensely grateful and inspired to have met researchers with such visible passion, fervent determination, and abundant kindness.

We have no conflicts of interest to disclose.

Correspondence regarding this thesis should be addressed to Erin Knape, Department of Psychology, University of Michigan, Ann Arbor, MI 48109. Email: eknape@umich.edu

Abstract

Neural distinctiveness and gamma-aminobutyric acid (GABA) have been proposed as critical drivers of age-related cognitive declines in older adults. The distinctiveness of neural activation patterns is commonly measured using functional magnetic resonance imaging (fMRI). However, fMRI is an indirect measure of neural activity with relatively poor temporal resolution. Electroencephalography (EEG) complements these limitations, as it is a direct measure with excellent temporal resolution. The current study tests whether a support vector machine (SVM) learning classifier can reliably measure EEG neural distinctiveness in the visual domain. EEG data from 27 healthy older adults (ages 65+) were collected during a "faces" versus "buildings" visual task. After preprocessing, we extracted 600 ms epochs starting at stimulus onset from all 64 electrodes and randomly divided these into training (90%) and testing (10%) datasets. We trained SVM classifiers with 20-fold cross-validation, and the most accurate model was used to classify the separate testing data. The classifiers demonstrated robust above-chance discrimination of face and building trials in the testing dataset, suggesting the potential viability of SVM classifiers as an EEG distinctiveness measure. We also investigated the relationship between EEG and fMRI distinctiveness, finding significant negative correlations when examining smaller fMRI regions of interest. Using magnetic resonance spectroscopy (MRS), we assessed whether EEG distinctiveness and fMRI distinctiveness are associated with GABA concentration. We did not find significant correlations, emphasizing the need for a larger sample size. This study offers insights into the unique contributions of neuroimaging modalities in investigating drivers of age-related cognitive decline.

Keywords: EEG, fMRI, neural distinctiveness, SVM, support vector machine, machine learning classifier

Investigating Visual Neural Distinctiveness through fMRI and EEG modalities using Support Vector Machine Classification

Aging is an indiscriminate and universal phenomenon often associated with cognitive performance declines, which can severely impair daily functioning and life quality (Cassady et al., 2020; Park et al., 2010; Salthouse, 1996). Mechanisms driving age-related cognitive decline have been proposed, including neural distinctiveness and gamma-aminobutyric acid (GABA), but these mechanisms are not fully understood (Lalwani et al., 2019; Park et al., 2010). The present study consolidated functional magnetic resonance imaging (fMRI) and electroencephalography (EEG) neuroimaging modalities, investigating what these approaches similarly and uniquely reveal about these drivers of age-related cognitive decline.

One proposed mechanism of cognitive decline is neural distinctiveness, in which stimuli from a specific category (e.g., faces) have specific neural patterns of activation that differ from those of other categories (e.g., houses) (Chamberlain et al., 2021). With age, it is hypothesized that neural representations become dedifferentiated, meaning neural representations of stimuli, such as faces versus houses, become more similar and, therefore, difficult to distinguish. Difficulty distinguishing stimuli may explain the cognitive performance impairments found among older adults (Simmonite & Polk, 2021).

Studies across multiple brain regions support this dedifferentiation hypothesis. Park et al. (2010) conducted behavioral tests and an fMRI visual task, finding that neural specificity (the level of distinctiveness) was predictive of fluid processing performance: Lower distinctiveness was associated with poorer fluid processing performance, and higher distinctiveness was associated with better fluid processing performance. The fMRI study by Lalwani et al. (2019) reinforces this result, finding that older adults had less distinctive neural activation patterns than

younger adults in the auditory cortex, making discerning between music and speech stimuli harder. Simmonite and Polk (2021) used fMRI to investigate neural distinctiveness across cortices, finding age-related decreases in distinctiveness in older adults compared to younger adults within the motor, auditory, and visual domains. Based on these studies, older adults tend to have dedifferentiated neural activation, leading to impaired cognitive performance.

Having established neural distinctiveness as a crucial mechanism of cognitive decline, GABA has been proposed as a driver of this phenomenon (Lalwani et al., 2019). GABA, an inhibitory neurotransmitter, resolves competition between neural representations, creating distinct activation patterns for different stimulus categories (Chamberlain et al., 2021). If GABA levels decrease with age, competing neural representations are not inhibited, resulting in less distinctive activation. Chamberlain et al. (2021) support this hypothesis, using magnetic resonance spectroscopy (MRS) to measure GABA and fMRI to estimate distinctiveness. Older adults were found to have lower GABA levels, and these were associated with less distinctive "face" versus "house" activation patterns. The critical work of fMRI and MRS studies suggests that GABA and neural distinctiveness contribute to age-related cognitive decline.

Although fMRI has become the standard measure of neural distinctiveness following its debut in the 1990s, this modality harbors notable limitations (Glover, 2011). This neuroimaging technique is a dynamic measure of metabolic activity. As brain regions become more active, blood flow increases to meet new oxygen requirements. fMRI detects the different magnetic properties of deoxygenated and oxygenated blood, providing a blood-oxygen-level-dependent (BOLD) signal, which indicates changes in brain activation during a scan. Because fMRI records the BOLD signal rather than neural activity, it is an indirect measure. Additionally, fMRI has poor temporal resolution, meaning changes in activation can be localized, but *when* these

changes occur after stimulus onset are less clear. Despite fMRI's advantages over other neuroimaging techniques (noninvasive with excellent spatial resolution), it falls short in directness and temporality.

This thesis consolidated the fMRI and EEG modalities to address the gaps in our understanding of neural distinctiveness and age-related cognitive decline. Pairing fMRI and EEG is beneficial, as EEG complements fMRI's limitations. While fMRI is indirect, EEG's scalp electrodes directly measure neural activity (Glover, 2011). Additionally, EEG has impressive temporal resolution (milliseconds) compared to fMRI's less precise rate (seconds). Our dataset is unique, as we have EEG and fMRI data from the same participants. In combination, fMRI localizes neural dedifferentiation within the brain and EEG identifies when this differentiation occurs. Leveraging our exceptional dataset, we explored the relation between these modalities and what they revealed about dedifferentiation.

Prior fMRI studies have used machine learning algorithms, such as support vector machines (SVMs), to measure neural distinctiveness. In 2010, Park et al. trained an SVM classifier to perform multivariate pattern analysis on visual task fMRI data. They defined neural distinctiveness as the accuracy with which the classifier predicts the correct stimulus category (faces versus houses) based on its associated neural activation pattern. This analysis was coarse due to the task's block design, meaning only a small number of activation patterns could be predicted. Despite this, researchers found that distinctiveness explained 30% of the variance of fluid processing ability. The use of SVM to explore fMRI data is valuable and well-documented (Lalwani et al., 2019; Park et al., 2010; Shahparian et al., 2019), but ceiling effects are a common issue. In contrast, the current study modeled EEG distinctiveness data, which contains more trials with more variability than is typical with fMRI data. Studies on wide-ranging cognitive topics

have demonstrated the successful use of SVM classifiers in analyzing EEG data (Amiri et al., 2022; Chan et al., 2011; Khatun et al., 2019). One notable study by Mahmud et al. (2020) examined the auditory functioning of older adults through a phoneme discrimination task in which participants distinguished between different auditory stimuli. SVM classifiers were used to classify the EEG recordings of hearing versus mildly impaired participants. This strong foundation suggests that SVM can be effectively adapted to measure EEG distinctiveness in the visual domain.

Given this background, our study explored what EEG and fMRI measures reveal about neural distinctiveness within the visual domain and how these modalities align and differ in the data they provide. Our first aim was to determine whether SVM classifiers can accurately classify faces versus buildings in an EEG visual task. We hypothesized that our trained models would perform significantly above chance (50% accuracy). This would provide backing for the use of SVM classification models as measures of EEG distinctiveness. Our second aim was to investigate the relationship between EEG and fMRI neural distinctiveness. We hypothesized that we would find a positive correlation in which participants with higher distinctiveness have both high EEG SVM classification accuracies and high fMRI distinctiveness scores. As previously mentioned, researchers have found an association between GABA concentration and fMRI neural distinctiveness, in which participants with lower GABA concentration exhibited less distinctive neural representations (Chamberlain et al., 2021). Our third aim examined whether this relationship is also found with EEG neural distinctiveness. We conducted a correlational analysis on GABA concentration and EEG SVM classification accuracies, hypothesizing a positive correlation. These findings would provide evidence for GABA as a potential mechanism of age-related neural dedifferentiation (Lalwani et al., 2019). With a more complete

understanding of how EEG and fMRI can be used in tandem, we can thoroughly investigate the mechanisms behind cognitive decline, leading to the development of treatments that abate these impairments and improve the lives of the older adult population.

Materials and Method

Participants

EEG data from 27 older adults, all 65 years old or older (mean age 70.96 yrs.; 16 females, 11 males), was obtained as part of the Michigan Neural Distinctiveness (MiND) study (Gagnon et al., 2019). MiND participants were recruited from and around Ann Arbor, Michigan, through the University of Michigan Health Research website (https://umhealthresearch.org) and community flyers advertising the study details. Following their completion of the main MiND study, older participants were contacted for an additional EEG data collection session. All MiND participants were native English speakers, right-handed, and psychologically and physically healthy. The Montreal Cognitive Assessment (MoCA) was administered to ensure all participants demonstrated healthy cognitive functioning. They were also screened for fMRI contraindications, such as foreign metallic objects or pacemakers, which would make the scan unsafe to perform. For full demographic information, see Table 1.

The MiND study received ethical approval from The University of Michigan Institutional Review Board (Study ID HUM00199054). Participants provided written consent before the EEG visual task was conducted (Study ID HUM00119987).

Table 1

Sociodemographic Characteristics of EEG Participants

Sample Characteristics	*n*	%	*M*	*SD*
Gender				
Women	16	59.259		
Men	11	40.741		
Age			70.963	5.66
Race				
Asian	1	3.704		
Black/African American	1	3.704		
Black/African American and White	2	7.407		
White	23	85.185		
Education (participant)				
High school or less	1	3.704		
Some college or associates	6	22.222		
Bachelors	6	22.222		
Advanced degree	14	51.852		
Education (mother)				
High school or less	15	55.556		
Some college or associates	7	25.926		
Bachelors	4	14.815		
Advanced degree	1	3.704		
MoCA Score			26.926	1.439
Visual Acuity			94.038	12.252

Note. n=27. Demographic characteristics of the EEG sample. “Advanced degree” includes master (MA), professional, Doctor of Medicine (MD), and Doctor of Philosophy (PhD) degrees. The Montreal Cognitive Assessment (MoCA) screens for mild cognitive impairment, evaluating domains such as attention, processing speed, and memory. The highest possible score is 30. The visual acuity uncorrected standard score assessed peripheral vision and ensured that individual differences in peripheral vision did not confound the visual neural distinctiveness results (Chamberlain et al., 2021).

Study Design

MiND Study

As part of the main MiND study, participants completed 2 hours of cognitive and behavioral tasks (Session 1), 45 minutes of behavioral tests, a 1-hour fMRI scan (Session 2), and an hour-and-a-half MRS scan (Session 3). Out of the initial 100 older adults, 27 participants in the current study returned for a 3-hour EEG session involving resting-state, auditory, and visual tasks. Our SVM analysis was conducted on the visual EEG task data.

Current Study

fMRI Data Acquisition.

fMRI data was acquired using a 3T GE MRI scanner at the University of Michigan's Functional Magnetic Resonance Imaging Laboratory. The blood-oxygen-level-dependent (BOLD) images were collected using a single-shot gradient echo (GRE) reverse spiral pulse sequence (TR = 2000 ms, TE = 30 ms, FOV = 220 mm, voxel size = 3.4375 × 3.4375 × 3 mm, 43 axial slices). High-resolution T1 images were acquired using an SPGR (3D BRAVO) sequence. Parameters: Inversion Time (TI) = 500 ms; flip angle = 15°; Field of View (FOV) = 256 × 256 mm; 1 × 1 × 1 mm voxels; 156 axial slices.

EEG Data Acquisition.

The EEG visual task was designed to best match the fMRI visual task while also being optimized to ensure high-quality EEG data. At the beginning of the session, 15 minutes were allotted to confirm participant consent and measure head size. The 44-minute visual task was conducted to measure EEG neural distinctiveness in the visual cortex. Participants wore a 64-electrode cap with silica gel applied to enhance electrode conductance (hair was not shaved).

Participants were asked to keep their eyes open, minimize muscle movements, and stare at a fixation cross.

Measures

fMRI Visual Task: Faces versus Buildings.

A six-minute fMRI run was administered to measure neural distinctiveness in the visual cortex. The fMRI run consisted of six 20-second house blocks and six 20-second face blocks presented in pseudorandom order with a 10-second fixation after each block. During a block, participants were presented with either grayscale face or house images. Each image (stimulus) was presented for 500 ms with a 500-ms interstimulus interval. During the face blocks, participants were presented with images of male faces and instructed to perform a right index finger button press whenever a female face (target image) was presented. During the house blocks, participants were presented with images of houses and instructed to perform a right index finger button press whenever an apartment (target image) was presented. Target images were displayed approximately once per minute. E-Prime 2.0 was used to present the stimuli, and a Lumina response pad from Cedrus was used to record participant responses during the task.

EEG Visual Task: Faces versus Buildings.

Eight blocks of grayscale house and face images were presented. Each block lasted about 4 min and 24 s (36 min total), with a break between the next. There were four conditions: male faces, female faces, houses, and apartments. In every block, participants were shown 176 images (44 male faces, 44 female faces, 44 houses, and 44 apartments). Each stimulus image was presented for 1.5 s (an image was displayed for 500 ms with a 750 ms fixation and 0-250 ms jitter). There were 40 regular trials and four catch trials within each condition. The catch trials (famous faces and buildings) were presented to ensure participants paid attention during the task.

The regular images were either male face or house images, and participants were instructed to press a button when a target image (female face or apartment building) was presented. See Figure 1 for stimuli examples.

Figure 1

EEG Visual Task Stimuli



Note. This figure depicts stimuli displayed during the EEG visual task. Examples of regular images (i.e., house and male face) are presented on the far left. Examples of target images (i.e., apartment and female face) are presented on the far right.

MRS: GABA Concentration Estimates.

MRS data was collected using the 3T GE MRI scanner at the University of Michigan's Functional Magnetic Resonance Imaging Laboratory. Estimates of GABA were obtained from two 3cm x 3cm x 3cm voxels placed in the ventral visual cortex using a MEGA-PRESS sequence. One voxel was placed in the left hemisphere, and the other voxel was placed in the right. Voxel placements were tailored to each participant based on the areas that had the highest activation during the fMRI visual task relative to their resting state condition. See Gagnon et al. (2019) for complete parameters. See Figure 2 for voxel placement examples.

Figure 2

MRS Voxel Placement

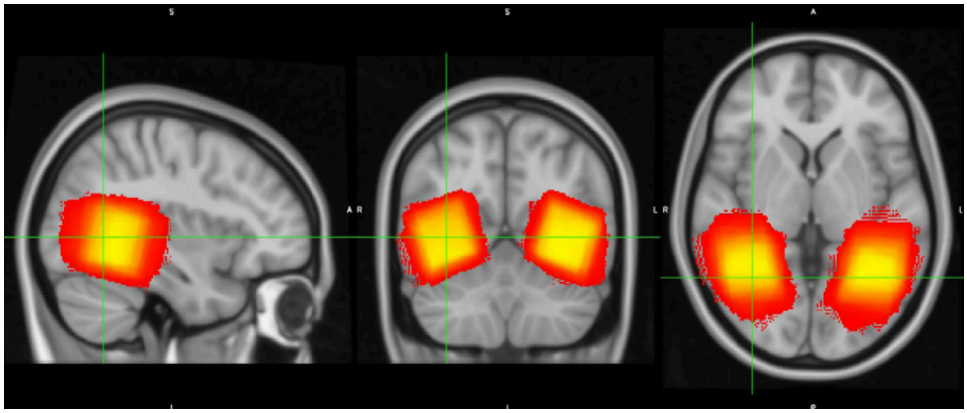

Note. The ventral visual cortex voxel placement across participants is depicted on the MNI T1 1-mm template. Darker colors (red) indicate less across-participant overlap. Brighter colors (yellow) indicate greater overlap. See Chamberlain et al.'s (2021) Figure 1 legend for more information.

Statistical Analysis

fMRI Preprocessing

Preprocessing steps, including physiological noise correction, slice-time correction, and motion correction, were performed using the RETROICOR algorithm (Brooks et al., 2008), SPM (University College London, n.d.), and FSL 5.0.7 (*FSL - FMRIB Software Library*, n.d.) (Chamberlain et al., 2021). FreeSurfer's recon-all function was used to reconstruct the structural image of each subject into two-dimensional cortical surfaces for each hemisphere, respectively (Laboratory for Computational Neuroimaging, n.d., version six). Each cortical surface's data was smoothed using a 5 mm FWHM kernel to reduce noise. The FsFast processing stream was then used to fit a general linear model to the fMRI time series at each vertex, describing how active each voxel was in response to face or house stimuli.

MRS Preprocessing

MEGA-PRESS data were analyzed using Gannet 3.3.2, a MATLAB software toolkit designed to analyze GABA-edited MRS data (Edden et al., 2014). Gannet utilized a Gaussian model to represent the GABA peak. Metabolite concentrations were then referenced to water. Using SPM12 segmentation, the GABA concentrations were corrected for cerebrospinal fluid (CSF) and the proportions of gray matter versus white matter within each voxel, resulting in uncorrected and tissue-corrected estimates. CSF and white matter have relatively low levels of GABA compared to grey matter. Corrections were conducted to account for these variations in GABA levels across different tissue types.

EEG Preprocessing

We preprocessed and analyzed the EEG data using EEGLAB, a MATLAB toolbox (MathWorks, Inc, Natick, Massachusetts, USA). To prepare for preprocessing, we downsampled the data from 5000Hz to 512Hz, which reduced the computational load. Channels 65 and above were removed, as they were blank. We applied a high pass filter (lower edge at 0.1Hz) and a low pass filter (100Hz) to remove low and high-frequency noise, respectively. “Bad” channels (those that remained flat for five or more seconds, were correlated less than .8 with nearby channels, or had larger amounts of line noise) were removed from the dataset. We then re-referenced to the average of all electrodes.

After re-referencing, 1200 ms epochs beginning 600 ms prior to stimulus onset and extending 600 ms after stimulus onset were extracted from all 64 electrodes. We performed Independent Component Analysis (ICA) on the data to separate artifacts from the neural signal. EEGLAB then flagged unwanted ICA components, reflecting muscle movements, eye blinks, and other artifacts. Trained researchers removed unwanted components (those labeled 90%

noise) following visual inspection. The data was then baseline corrected using the -600 to 0 ms pre-stimulus period as the baseline. To ensure consistency in the number of channels, values from "good" EEG channels were interpolated, replacing the channels that were removed at earlier preprocessing stages. The data was then re-referenced to the average, resulting in 64 channels. Lastly, we used a moving window peak-to-peak artifact detection and rejection tool to flag and remove epochs that contained artifacts after preprocessing. Specifically, epochs containing signal fluctuations of greater than 200mV within 200 ms were removed. Standardization of the remaining EEG data was conducted to ensure every participant had equivalent training and testing data to be analyzed.

Data Quality

Prior to conducting statistical analyses on the MRS data, we estimated GABA fit error using Gannet 3.3.2 and visual inspection, ensuring the estimated values were below 15% (goodness of model fit). Regarding behavior analysis, we excluded outliers (three SDs above the mean) to avoid measurement error.

fMRI: Calculating Neural Distinctiveness

Multivariate pattern analysis (MVPA) was used to assess fMRI neural distinctiveness within functional regions of interest (ROIs) (Gagnon et al., 2019). FsFast provided estimates of the neural responses. A block design with separate regressors was used to model the two visual conditions (faces versus houses). Anatomical masks for the visual task were obtained with FreeSurfer and were used to create a functional ROI for each participant. See Figure 3 for an example of an ROI visualization.

Within the ROI, we calculated within-condition correlations (how similar the neural activation patterns are across every combination of face block pairs; how similar the neural

activation patterns are across every combination of house block pairs) and averaged. We also calculated between-condition correlations (how similar are the "house" activation patterns to the "face" activation patterns) and averaged. fMRI neural distinctiveness was calculated by subtracting the average within-condition correlation (the average correlation between all house pairs and all face pairs) from the between-condition correlation (the average correlation of all house-face pairs) (Chamberlain et al., 2021). A participant with distinctive face versus house representations would have high within-condition and low between-condition correlations, meaning the participant would have a value closer to +2 than -2.

Figure 3

fMRI ROI

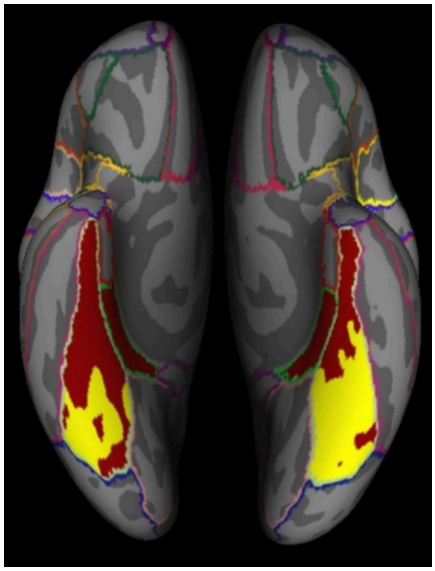

Note. An example of ventral visual functional (yellow) and structural (red) fMRI regions of interest (ROIs) acquired from a participant. The 5000 most activated vertices during the house and face conditions were used to create the functional ROI. See Chamberlain et al.'s (2021) Figure 2 legend for more information.

EEG: Calculating Neural Distinctiveness using Support Vector Machine (SVM) Classifiers

Following preprocessing, we extracted the EEG time series from EEGLAB as a matrix (electrode x time point x trial). Time points prior to stimulus presentation were discarded, while data from 0 ms to 600 ms (with respect to stimulus presentation) were retained. The data matrix was reshaped into a 2D matrix by concatenating the data from each electrode. This resulted in a matrix with one row per trial, with this row containing the data from all electrodes. We then created a separate array labeling whether each row of the matrix reflected a face trial (coded as 1) or a house trial (coded as 2).

Each participant's EEG data were randomly divided into training (90%) and testing (10%) datasets. Two approaches were taken for model training. First, a standard SVM classifier was trained on the entire training dataset to differentiate face and house images based on the participant's EEG time series patterns. Second, 20-fold cross-validation was employed (the training data was further divided into 20 equal parts, or 'folds'). Then, SVM classifiers were trained and evaluated 20 separate times. In each iteration, 19 of the 20 folds were used as the training set, and the 20th was used as the validation set to evaluate the model's performance. The most accurate model across the 20 folds was selected as the cross-validated model. Both the standard model and the cross-validated model were used to predict the labels (faces or houses) of the testing data. Then, the classification accuracies (whether the trained models predicted the correct labels) were calculated. If trained on a participant with low distinctiveness, the algorithm would be unable to classify the neural activation patterns for faces versus houses, resulting in lower classification accuracy. As the models were presented with a two-condition ("face" versus "house") classification problem, 50% accuracy represents chance-level performance. If trained on a participant with high distinctiveness, the algorithm would accurately classify the neural

activation patterns. Thus, the standard and cross-validated models provide a means of assessing the distinctiveness of EEG responses elicited by each condition.

Results

One participant lacked data after ICA artifact removal. They were excluded from the analyses presented in the results section. Regarding the MRS data, the uncorrected and tissue-corrected data in the left ventral visual cortex for one participant was not collected due to technical issues.

Aim 1: Can SVM models successfully classify faces versus buildings as a measure of visual EEG neural distinctiveness?

The SVM classifiers demonstrated robust discrimination of the "face" versus "house" neural activation patterns provided by the testing dataset. We conducted a one-sample t-test comparing the classification accuracy values of the SVM Standard Model with chance (50%). This test indicated that the mean (M = 94.46%, SD = 2.89%) was significantly greater than 50%, showing that the Standard Model can accurately classify visual stimuli belonging to different categories ($t(25) = 78.508$, $p < .0001$). We conducted an additional one-sample t-test comparing the classification accuracy values of the SVM 20-fold cross-validation with chance (50%). Again, the mean (M = 87.56%, SD = 5.89%) was significantly greater than 50%, displaying the model's ability to accurately classify visual stimuli ($t(25) = 75.408$, $p < .0001$). Although the SVM Standard Model was more accurate, this model runs the risk of overfitting, making the 20-fold cross-validation the preferred model for novel data (GeeksforGeeks, 2024). Based on these accuracies, we conclude that SVM models can be used to successfully classify EEG neural distinctiveness data in the visual domain.

Aim 2: Are EEG and fMRI neural distinctiveness correlated?

To examine whether EEG visual distinctiveness is related to fMRI visual distinctiveness, we conducted a Pearson correlation analysis. We first explored the association between the EEG SVM Standard Model classification accuracies and fMRI neural distinctiveness scores. We found stronger correlations between EEG and fMRI when using smaller fMRI ROIs. The correlations for the ROIs with 50 ($r(24) = -.52$, $p = .007$), 100 ($r(24) = -.47$, $p = .02$) and 200 vertices ($r(24) = -.40$, $p = .04$) were statistically significant. The correlation for the ROI with 300 vertices was not statistically significant but could be interpreted as marginally significant ($r(24) = -.36$, $p = .07$). The correlations for the ROIs with 400 ($r(24) = -.31$, $p = .12$), 600 ($r(24) = -.26$, $p = .21$), 1000 ($r(24) = -.22$, $p = .28$), 2000 ($r(24) =-.21$, $p = .30$), 5000 ($r(24) = -.16$, $p = .44$), and 10000 vertices ($r(24) = -.10$, $p = .63$) were not statistically significant. It is notable that these correlations are negative, as this contradicts our hypothesis that the level of distinctiveness aligns across neuroimaging modalities.

The association between EEG SVM 20-fold cross-validation and the fMRI neural distinctiveness scores followed a similar trend (stronger correlations with smaller ROIs) but showed weaker correlations overall. For the ROI with 50 vertices, the correlation was statistically significant ($r(24) = -.41$, $p = .04$). Figure 4 illustrates this correlation. The correlation for the ROI with 100 vertices was not statistically significant but could be interpreted as marginally significant ($r(24) = -.34$, $p = .09$). The correlations for ROIs with 200 ($r(24) = -.24$, $p = .24$), 300 ($r(24) = -.18$, $p = .37$), 400 ($r(24) = -.13$, $p = .54$), and 600 vertices ($r(24) = -.07$, $p = .73$) were not statistically significant. Additionally, the correlations for ROIs with 1000 ($r(24) = -.03$, $p = .88$), 2000 ($r(24) = -.03$, $p = .88$), 5000 ($r(24) = .04$, $p = .85$), and 10000 ($r(24) = .09$, $p = .65$) were not statistically significant. See Figure 5 for a scatterplot examining an ROI of 200

vertices. See Figure 6 for a scatterplot examining an ROI of 5000 vertices. For full results, see Table A1.

Figure 4

Scatterplot of EEG Cross-validation versus fMRI distinctiveness

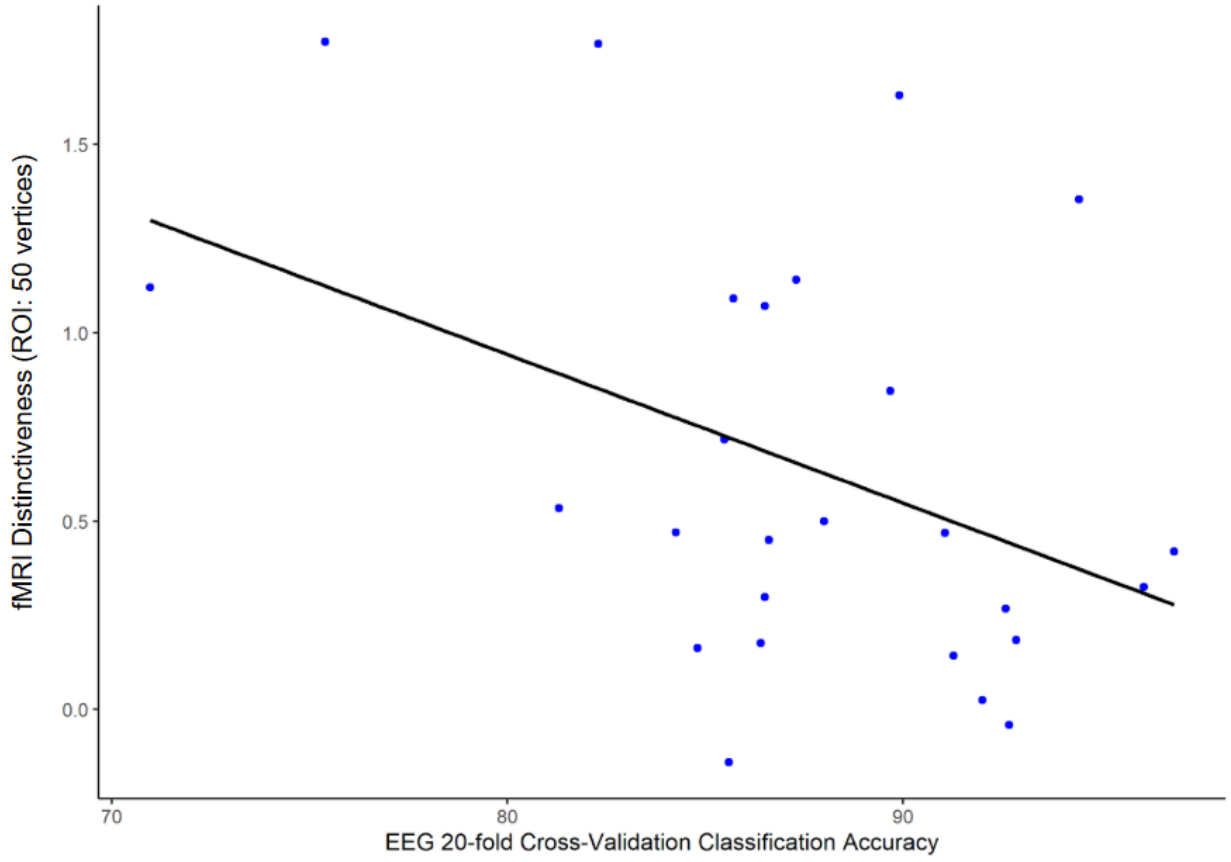

Figure 5

Scatterplot of EEG Cross-validation versus fMRI distinctiveness

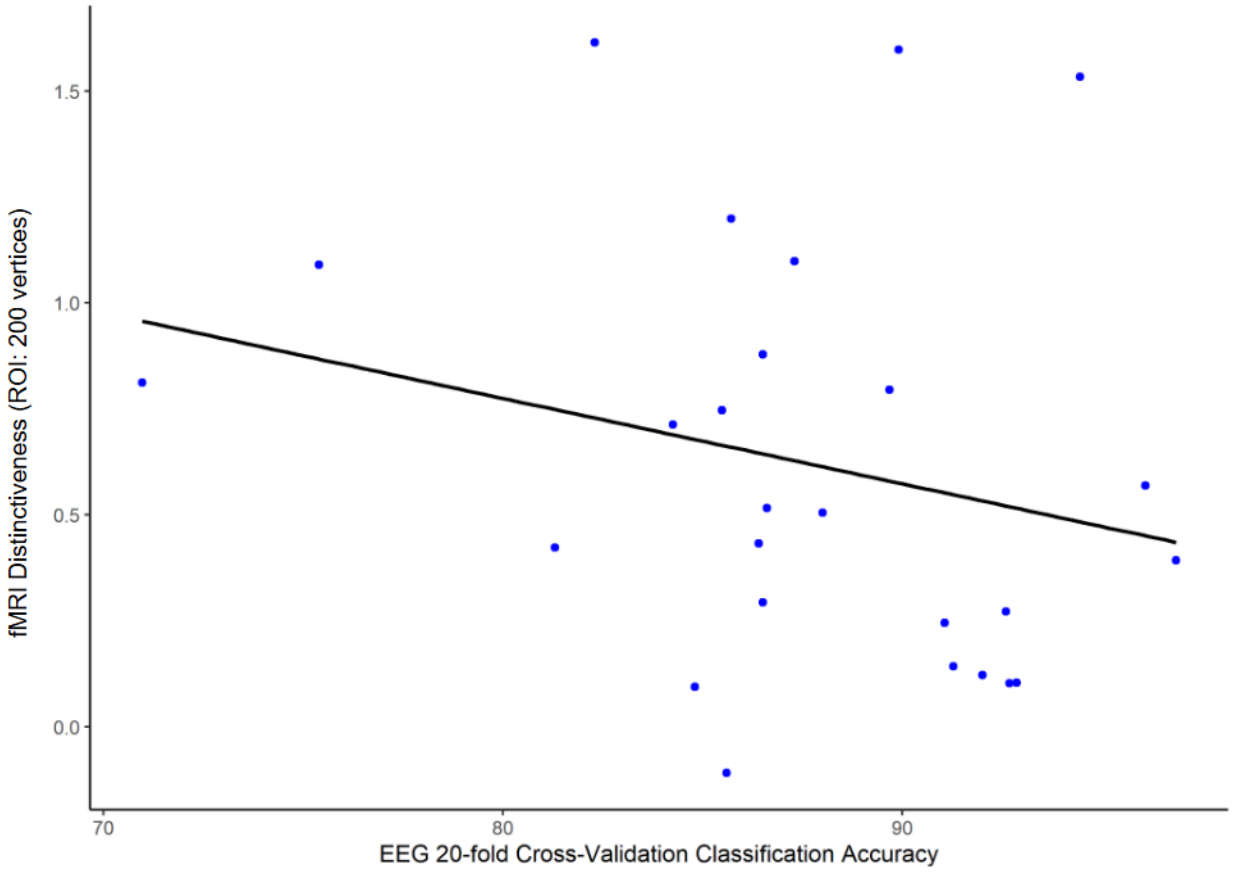

Figure 6

Scatterplot of EEG Cross-validation versus fMRI distinctiveness

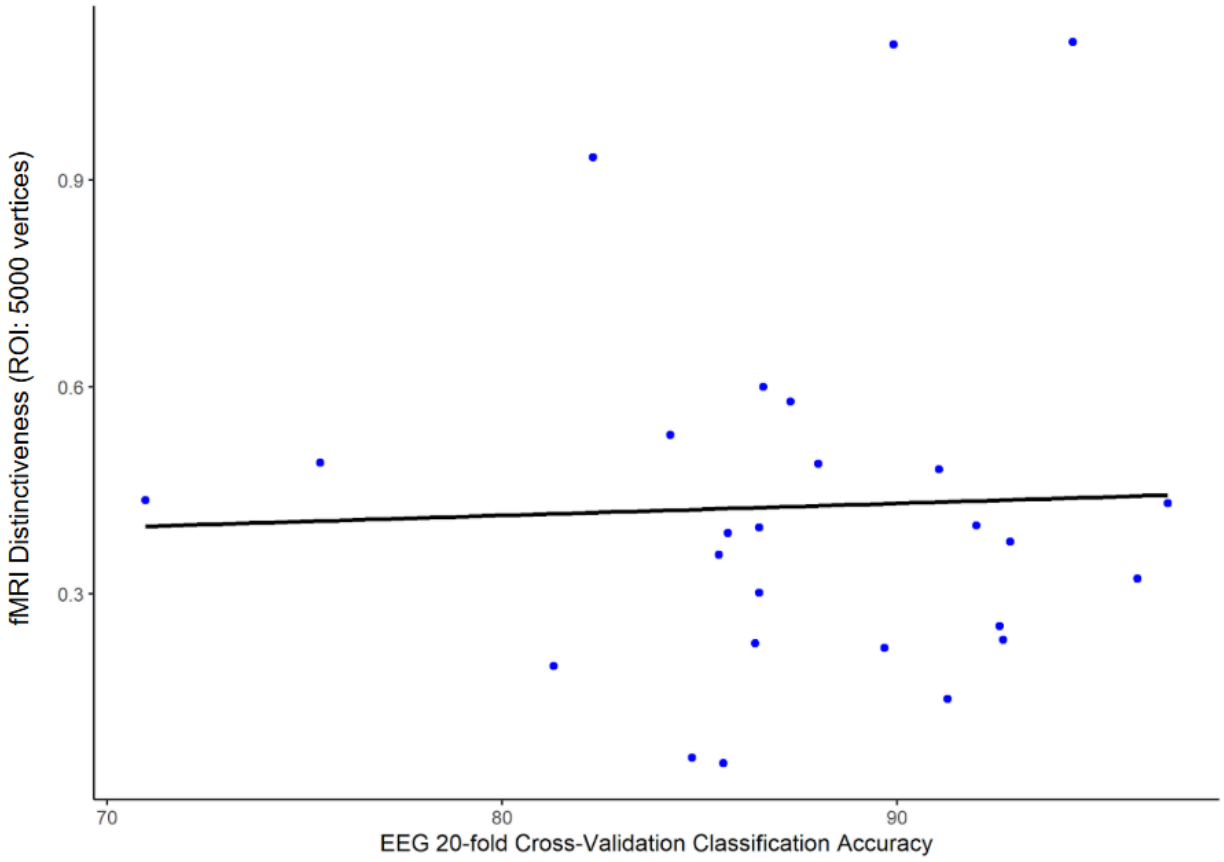

Aim 3: Is GABA concentration correlated with EEG distinctiveness as measured by SVM?

We explored relationships between EEG classification accuracies and GABA concentrations in the visual cortex using Pearson's correlations. We calculated the correlations between the EEG SVM Standard Model accuracy values and uncorrected and tissue-corrected GABA concentrations. The correlations for tissue-corrected in the left ($r(23) = .13$, $p = .53$) and right ($r(24) = .16$, $p = .43$) ventral visual cortex and uncorrected in the left ventral visual cortex ($r(23) = .20$, $p = .35$) were not statistically significant. The strongest correlation was between the Standard Model and uncorrected GABA in the right ventral visual cortex, but this was not statistically significant ($r(24) = .29$, $p = .15$).

This trend was also found when correlating the EEG SVM 20-fold cross-validation accuracies and GABA concentrations. The correlations for tissue-corrected in the left ($r(23) = .13$, $p = .55$) and right ($r(24) = .07$, $p = .72$) ventral visual cortex and uncorrected in the left ventral visual cortex ($r(23) = .16$, $p = .44$) were not statistically significant. Again, uncorrected GABA in the right ventral visual cortex displayed the strongest correlation, but this was not statistically significant ($r(24) = .21$, $p = .30$). Figure 7 illustrates this correlation. See Table A2 for full results.

Although we did not observe a significant relationship between EEG and GABA, Chamberlain et al. (2021) found a significant relationship between fMRI and GABA with a larger sample. Based on this previous finding, we conducted an exploratory analysis assessing whether GABA concentration and fMRI neural distinctiveness are correlated. The same Pearson correlation method was applied. The correlations with the fMRI neural distinctiveness scores were not statistically significant, following the same trend observed with the EEG data. To illustrate, the correlations between the ROI with 50 vertices and the uncorrected ($r(23) = .08$, $p = .70$) and tissue corrected ($r(23) = .05$, $p = .81$) GABA concentrations in the left ventral visual cortex were not statistically significant. For the ROI with 5000 vertices, the uncorrected ($r(23) = -.10$, $p = .64$) and tissue corrected ($r(23) = -.10$, $p = .63$) GABA concentrations in the left ventral visual cortex were also not statistically significant. The strongest correlation was between the ROI containing 200 vertices and the uncorrected GABA in the right ventral visual cortex ($r(24) = .26$, $p = .20$). This correlation was not statistically significant and is represented in Figure 8. For full results, see Table A3.

As a part of the exploratory analysis, we compared the strength of the relationships between GABA and EEG versus GABA and fMRI. Specifically, we assessed whether the

correlations of EEG 20-fold cross-validation accuracies and GABA (r(24) = .21, p = .30) and fMRI distinctiveness scores (ROI: 200 vertices) and GABA (r(24) = .26, p = .20) are significantly different. The uncorrected GABA in the right ventral visual cortex was used for this analysis, as it provided the strongest correlations. Williams's t-test (1959) was conducted, and the results indicated no statistically significant difference between the two correlations (t(22) = -.18, p = .86, 95% CI [-0.56, 0.46]). Because these correlations are similar in strength, a larger sample size may uncover significant relationships across both neuroimaging modalities.

Figure 7

Scatterplot of EEG Cross-validation versus GABA Concentration

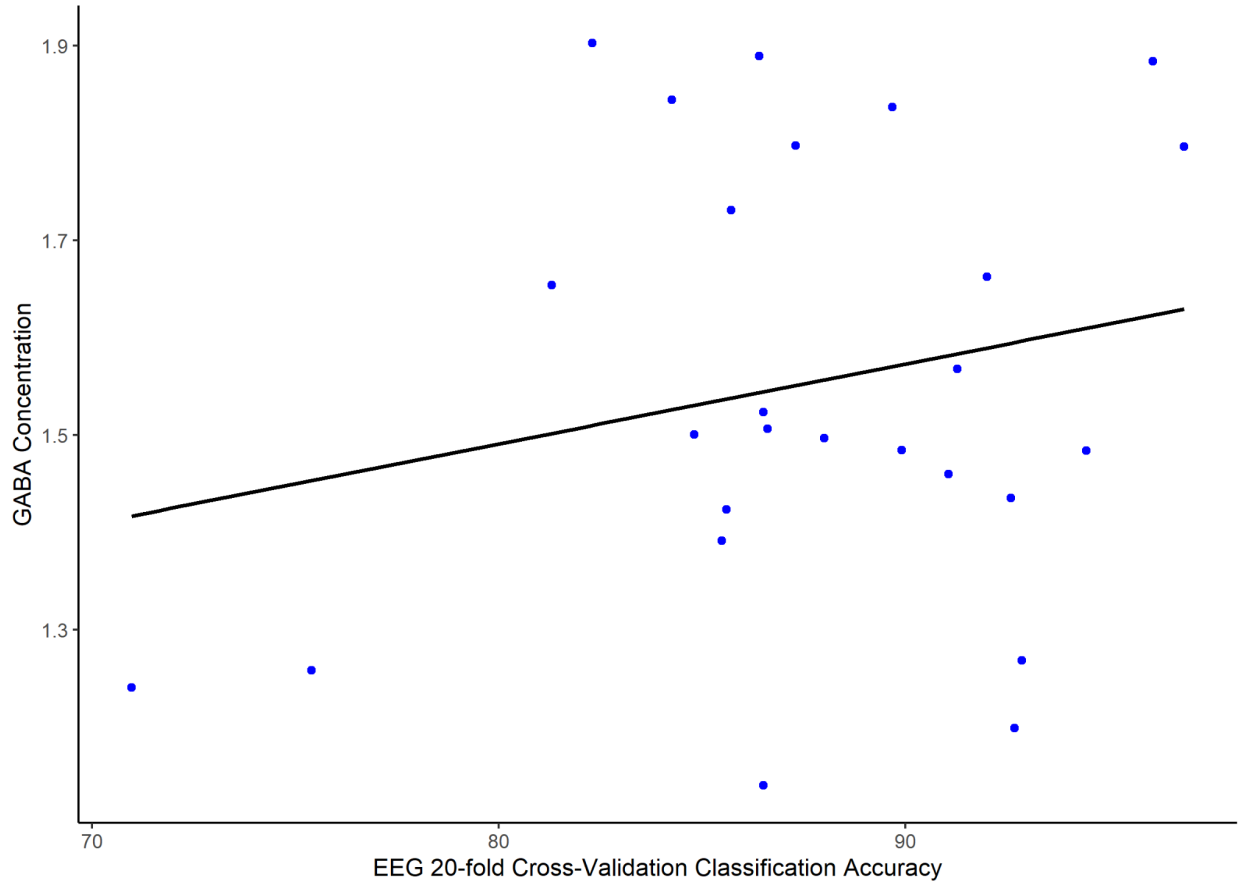

Note. Uncorrected GABA concentration in the right ventral visual area.

Figure 8

Scatterplot of fMRI Distinctiveness versus GABA Concentration

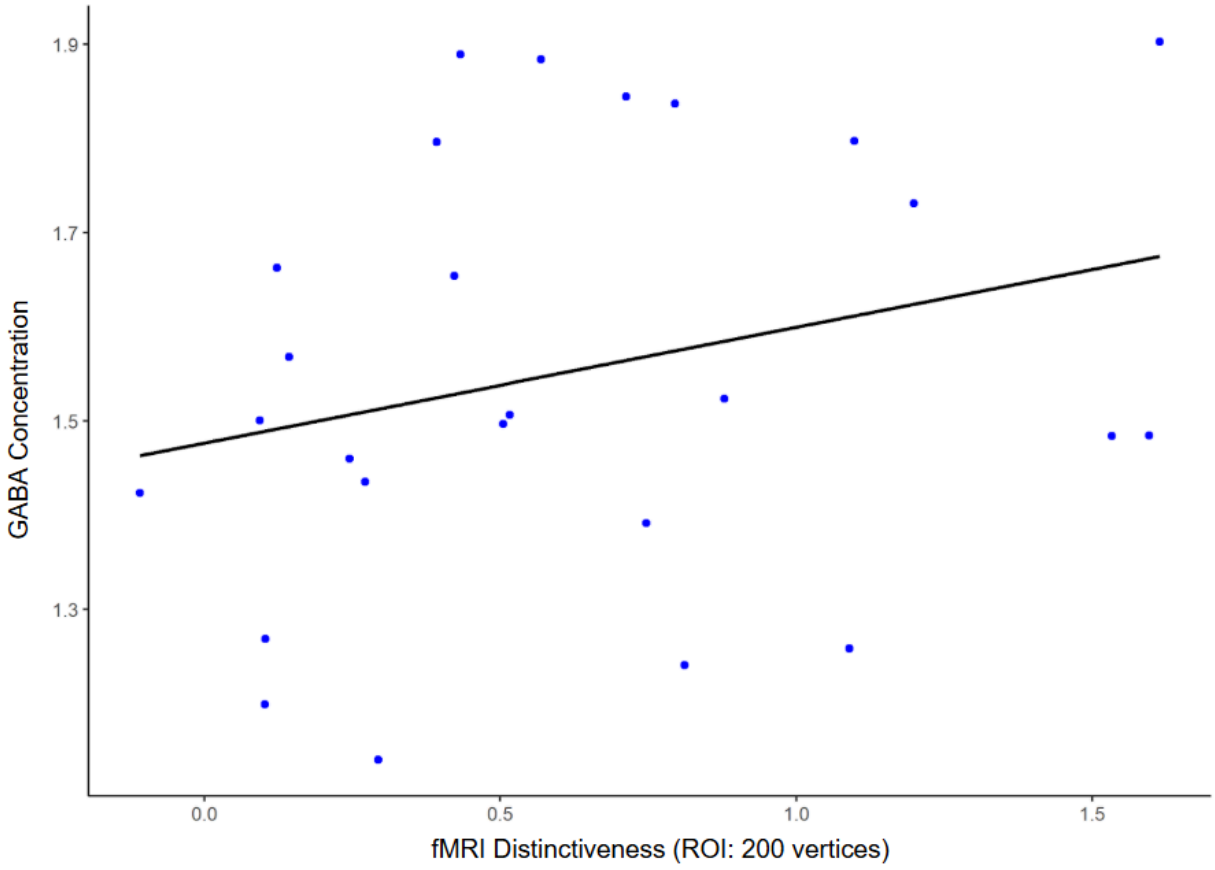

Note. Uncorrected GABA concentration in the right ventral visual area.

Discussion

The present study aimed to examine neural distinctiveness and GABA concentrations in the visual cortex using both EEG and fMRI neuroimaging modalities. We successfully used SVM classifiers to distinguish between stimulus categories in EEG data. We also found correlations between EEG classification accuracy and fMRI measures of distinctiveness. By joining these complementary neuroimaging techniques, we can deepen our understanding of the mechanisms driving age-related cognitive decline.

Our study found that SVM classification models can accurately classify “house” versus “face” stimuli. Our standard and 20-fold cross-validation SVM models demonstrated robust above-chance (50%) discrimination of house and face trials in the testing dataset. This finding is supported by previous research utilizing SVM learning models to classify and decode EEG data (Amiri et al., 2022; Chan et al., 2011; Khatun et al., 2019; Mahmud et al., 2020). Our results highlight the viability of SVM classifiers as a measurement of visual neural distinctiveness for EEG data. Training our models on participants with low distinctiveness would yield lower classification accuracies. Training our models on participants with high distinctiveness would yield higher classification accuracies. Thus, SVM models have excellent potential for future EEG neural distinctiveness studies.

Our study also investigated whether there is a correlation between EEG neural distinctiveness (as measured by SVM) and fMRI neural distinctiveness. We anticipated a positive relationship between fMRI distinctiveness scores and the EEG standard and 20-fold cross-validation SVM models. However, our findings indicated a negative relationship, in which participants with higher EEG distinctiveness had lower fMRI distinctiveness and vice versa. Differences in the EEG and fMRI neural distinctiveness measures could explain these unexpected results. Although the EEG visual task was designed to best match the fMRI visual task, they were not perfectly equivalent. The EEG task was 45 min in duration, whereas the fMRI task spanned 6 min. The EEG task was also event-related, whereas the fMRI task was administered in a block design. The manner of data collection also differed. The EEG electrode cap collected data from the whole brain, while the fMRI measure included only visual cortex vertices. These measurement-based differences may have contributed to our unexpected findings.

Another potential driver behind this anticorrelation is compensatory recruitment. Reuter-Lorenz and Cappell (2008) discuss the theory of age-related compensatory overactivation, in which older adults exhibit greater neural activation than younger adults to compensate for cognitive deficiencies and maintain high performance. They propose that these cognitive deficiencies may be related to "representational codes" becoming "less specific" with age, requiring greater activation within certain brain regions (p. 179). Applying this to the current study, it is possible that older adults with lower distinctiveness (more confusable neural representations) in the most task-relevant voxels also exhibit diffuse compensatory activity. Our EEG data was acquired from the entire brain, meaning the signals collected and used by the SVM classifiers may have been influenced by this activity. This hypothesis is supported by our findings that the strongest correlations between EEG and fMRI distinctiveness were found with the smallest ROIs, which are the most distinct. Acquiring EEG data from a smaller subset of electrodes may circumvent this compensatory activity and reveal a positive correlation between EEG and fMRI distinctiveness.

Despite the negative direction of our correlations, we did find a significant relationship between EEG and fMRI neural distinctiveness. The EEG SVM standard model correlated more strongly than the 20-fold cross-validation model. This was expected, as the standard model is overfitted to the dataset (GeeksforGeeks, 2024). Notably, statistically significant correlations were found only with smaller ROI sizes, which contained fewer vertices. For instance, ROIs with 50 vertices produced stronger correlations than those with 2000. Lalwani et al. (2019) found a similar finding in which distinctiveness diminished as the size of ROIs increased. They proposed that larger ROIs contain noise and unrelated activity. Therefore, the dilution of our EEG and fMRI distinctiveness correlations may be due to the irrelevant data present in larger ROIs.

Overall, these findings suggest a relationship between EEG and fMRI, but more work is needed to determine the nature of this relationship.

Prior research has found associations between GABA concentration and fMRI neural distinctiveness, whereby participants with higher GABA concentrations had higher distinctiveness (Chamberlain et al., 2021). Surprisingly, our study did not find significant correlations between GABA concentration and EEG neural distinctiveness with the standard or 20-fold cross-validation SVM models. This could be attributed to differences in directness, temporality, and spatial resolution across neuroimaging techniques (Glover, 2011) or unforeseen differences across the EEG and fMRI visual tasks. However, our correlation comparison implicates a different problem. Rather than one neuroimaging modality displaying a stronger correlation with GABA than the other, these correlations were similar in strength ($r = \sim .235$), suggesting a power issue. Our sample size (n=26 after preprocessing) is small, meaning there may be a significant correlation, but we lacked the power to detect it. Chamberlain et al. (2021) found a significant relationship between fMRI and GABA in a sample of 51 older adults. With increased power, we may have observed significant relationships between GABA concentrations and our EEG distinctiveness measure.

This study provides a foundation for future neural distinctiveness and GABA investigations utilizing EEG and fMRI modalities. Our project displays the utility of SVM in successfully classifying EEG visual data. These neuroimaging techniques can also be correlated, and although the correlations between EEG and GABA were not significant, additional research with a larger sample may reveal stronger associations. This project is an important step in identifying how different neuroimaging techniques can be consolidated to reveal new insights into human cognition. Achieving a more thorough understanding of the mechanisms behind

age-related cognitive decline will motivate and inform the development of interventions to improve the quality of life of cognitively impaired older adults.

Limitations and Future Work

Future research should address the limitations of our study. Only 27 of the initial 100 older adults from the MiND project returned for an EEG session, and only 26 were included in the analysis. Acquiring a larger sample size would increase our statistical power, making it possible to detect more subtle but statistically significant correlations between EEG and fMRI distinctiveness measures and GABA that are not evident in this study. A larger sample size may also clarify the direction of the EEG and fMRI associations. Additional work using a smaller number of EEG electrodes or a single electrode may shed light on compensatory overactivation as a cause of the anticorrelation found in the present study. Our analyses were also correlational. Future studies should determine whether there is a causal relationship between GABA and EEG distinctiveness. These results would provide evidence that age-related decreases in GABA hinder the creation of distinct activation patterns, resulting in cognitive decline (Chamberlain et al., 2021). As mentioned previously, EEG complements fMRI's limitations, specifically regarding temporality (Glover, 2011). Future work should explore how the relationship between fMRI and EEG distinctiveness changes across EEG time windows (epochs). These epochs account for different levels of cognitive processing (e.g., visual perception versus higher cognitive functions). Identifying how these neuroimaging techniques capture the complexities of neural functioning could provide deeper insights into the drivers of cognitive decline. Lastly, the current study examined cognition only within the ventral visual cortex. Future work should explore the relationship between GABA, fMRI distinctiveness, and EEG distinctiveness within the auditory and motor cortical areas to better understand how the brain changes with age.

Conclusion

In closing, our findings display the promise of SVM classifiers as measures of EEG neural distinctiveness in the visual cortex. Additionally, we found significant correlations between EEG and fMRI neural distinctiveness. Future work should explore this relationship and its direction to identify what these neuroimaging techniques similarly and uniquely reveal about cognition. Although we did not find significant correlations between GABA and EEG neural distinctiveness, this highlights the importance of acquiring larger sample sizes for future studies. Together, our results provide a solid foundation for exploring the mechanisms behind age-related cognitive decline. These and future research efforts will inform the development of treatments and interventions that transform the lives of those experiencing cognitive impairment.

References

Amiri, M., Fisher, P. M., Raimondo, F., Sidaros, A., Hribljan, M. C., Othman, M. H., Zibrandtsen, I., Albrechtsen, S. S., Bergdal, O., Hansen, A. E., Hassager, C., Højgaard, J. L. S., Jakobsen, E. W., Jensen, H. R., Møller, J., Nersesjan, V., Nikolic, M., Olsen, M. H., Sigurdsson, S. T., . . . Kondziella, D. (2022). Multimodal prediction of residual consciousness in the intensive care unit: The CONNECT-ME study. *Brain*, *146*(1), 50–64. https://doi.org/10.1093/brain/awac335

Brooks, J. C., Beckmann, C. F., Miller, K. L., Wise, R. G., Porro, C. A., Tracey, I., & Jenkinson, M. (2008). Physiological noise modeling for spinal functional magnetic resonance imaging studies. *NeuroImage*, *39*(2), 680–692. https://doi.org/10.1016/j.neuroimage.2007.09.018

Cassady, K., Ruitenberg, M. F. L., Reuter-Lorenz, P. A., Tommerdahl, M., & Seidler, R. D. (2020). Neural Dedifferentiation across the lifespan in the motor and somatosensory systems. *Cerebral Cortex*, *30*(6), 3704–3716. https://doi.org/10.1093/cercor/bhz336

Chamberlain, J. D., Gagnon, H., Lalwani, P., Cassady, K. E., Simmonite, M., Seidler, R. D., Taylor, S. F., Weissman, D. H., Park, D. C., & Polk, T. A. (2021). GABA levels in ventral visual cortex decline with age and are associated with neural distinctiveness. *Neurobiology of Aging*, *102*, 170–177. https://doi.org/10.1016/j.neurobiolaging.2021.02.013

Chan, A. M., Halgren, E., Marinkovic, K., & Cash, S. S. (2011). Decoding word and category-specific spatiotemporal representations from MEG and EEG. *NeuroImage*, *54*(4), 3028–3039. https://doi.org/10.1016/j.neuroimage.2010.10.073

Diedenhofen, B., & Musch, J. (2015). cocor: A Comprehensive Solution for the Statistical Comparison of Correlations. *PLoS ONE*, *10*(4), e0121945. https://doi.org/10.1371/journal.pone.0121945

Edden, R. A., Puts, N. A., Harris, A. D., Barker, P. B., & Evans, C. J. (2014). Gannet: A batch‐processing tool for the quantitative analysis of gamma‐aminobutyric acid–edited MR spectroscopy spectra. *Journal of Magnetic Resonance Imaging*, *40*(6), 1445–1452. https://doi.org/10.1002/jmri.24478

FSL - FMRIB Software Library. (n.d.). https://www.fmrib.ox.ac.uk/fsl

Gagnon, H., Simmonite, M., Cassady, K., Chamberlain, J., Freiburger, E., Lalwani, P., Kelley, S., Foerster, B., Park, D. C., Petrou, M., Seidler, R., Taylor, S. F., Weissman, D. H., & Polk, T. A. (2019). Michigan Neural Distinctiveness (MiND) study protocol: Investigating the scope, causes, and consequences of age-related neural dedifferentiation. *BMC Neurology*, *19*(1). https://doi.org/10.1186/s12883-019-1294-6

GeeksforGeeks. (2024, April 2). *How K-Fold Prevents overfitting in a model?* https://www.geeksforgeeks.org/how-k-fold-prevents-overfitting-in-a-model/

Glover, G. H. (2011). Overview of functional magnetic resonance imaging. *Neurosurgery Clinics of North America*, *22*(2), 133–139. https://doi.org/10.1016/j.nec.2010.11.001

Khatun, S., Morshed, B. I., & Bidelman, G. M. (2019). A single-channel EEG-based approach to detect mild cognitive impairment via speech-evoked brain responses. *IEEE Transactions on Neural Systems and Rehabilitation Engineering*, *27*(5), 1063–1070. https://doi.org/10.1109/tnsre.2019.2911970

Laboratory for Computational Neuroimaging. (n.d.). *FreeSurfer*. FreeSurfer. https://surfer.nmr.mgh.harvard.edu/

Lalwani, P., Gagnon, H., Cassady, K., Simmonite, M., Peltier, S., Seidler, R. D., Taylor, S. F., Weissman, D. H., & Polk, T. A. (2019). Neural distinctiveness declines with age in auditory cortex and is associated with auditory GABA levels. *NeuroImage*, *201*, 116033. https://doi.org/10.1016/j.neuroimage.2019.116033

Mahmud, M. S., Ahmed, F., Al-Fahad, R., Moinuddin, K. A., Yeasin, M., Alain, C., & Bidelman, G. M. (2020). Decoding Hearing-Related changes in older adults' spatiotemporal neural processing of speech using machine learning. *Frontiers in Neuroscience*, *14*. https://doi.org/10.3389/fnins.2020.00748

Park, J., Carp, J., Hebrank, A., Park, D., & Polk, T. (2010). Neural specificity predicts fluid processing ability in older adults. *The Journal of Neuroscience*, *30*(27), 9253–9259. https://doi.org/10.1523/jneurosci.0853-10.2010

Reuter-Lorenz, P. A., & Cappell, K. A. (2008). Neurocognitive aging and the compensation hypothesis. *Current Directions in Psychological Science*, *17*(3), 177–182. https://doi.org/10.1111/j.1467-8721.2008.00570.x

Salthouse, T. A. (1996). The processing-speed theory of adult age differences in cognition. *Psychological Review*, *103*(3), 403–428. https://doi.org/10.1037/0033-295x.103.3.403

Shahparian, N., Yazdi, M., & Khosravi, M. R. (2019). Alzheimer disease diagnosis from fMRI images based on latent low rank features and Support Vector Machine (SVM). *Current Signal Transduction Therapy*, *16*(2), 171–177. https://doi.org/10.2174/1574362414666191202144116

Simmonite, M., & Polk, T. A. (2021). Age-related declines in neural distinctiveness correlate across brain areas and result from both decreased reliability and increased confusability.

Aging Neuropsychology and Cognition, *29*(3), 483–499.

https://doi.org/10.1080/13825585.2021.1999383

University College London. (n.d.). *Statistical Parametric Mapping*. Functional Imaging Laboratory. https://www.fil.ion.ucl.ac.uk/spm/

Appendix

Complete Correlation Results Tables

Table A1

Correlations between EEG and fMRI measures of neural distinctiveness

SVM Model	ROI size (vertices)	r	df	p-value
Standard	50	-.52	24	<.01
Standard	100	-.47	24	.02
Standard	200	-.40	24	.04
Standard	300	-.36	24	.07
Standard	400	-.31	24	.12
Standard	600	-.26	24	.21
Standard	1000	-.22	24	.28
Standard	2000	-.21	24	.30
Standard	5000	-.16	24	.44
Standard	10000	-.10	24	.63
20foldCrossValid	50	-.41	24	.04
20foldCrossValid	100	-.34	24	.09
20foldCrossValid	200	-.24	24	.24
20foldCrossValid	300	-.18	24	.37
20foldCrossValid	400	-.13	24	.54
20foldCrossValid	600	-.07	24	.73
20foldCrossValid	1000	-.03	24	.88
20foldCrossValid	2000	-.03	24	.88
20foldCrossValid	5000	.04	24	.85
20foldCrossValid	10000	.09	24	.65

Note. This table displays correlations between all fMRI distinctiveness scores and the standard and 20-fold cross-validation EEG SVM models. ROI: region of interest.

Table A2

Correlations between EEG neural distinctiveness and GABA concentrations

SVM Model	MRS Tissue Correction Type	GABA Voxel Location	r	df	p-value
Standard	Uncorrected	Left ventral visual	.20	23	.35
Standard	Tissue-corrected	Left ventral visual	.13	23	.53
Standard	Uncorrected	Right ventral visual	.29	24	.15
Standard	Tissue-corrected	Right ventral visual	.16	24	.43
20foldCrossValid	Uncorrected	Left ventral visual	.16	23	.44
20foldCrossValid	Tissue-corrected	Left ventral visual	.13	23	.55
20foldCrossValid	Uncorrected	Right ventral visual	.21	24	.30
20foldCrossValid	Tissue-corrected	Right ventral visual	.07	24	.72

Note. This table displays correlations between GABA concentrations and the standard and 20-fold cross-validation EEG SVM models.

Table A3

Correlations between fMRI neural distinctiveness and GABA concentrations

ROI size (vertices)	MRS Tissue Correction Type	GABA Voxel Location	r	df	p-value
50	Uncorrected	Left ventral visual	.08	23	.70
50	Uncorrected	Right ventral visual	.09	24	.66
200	Uncorrected	Left ventral visual	.11	23	.60
200	Uncorrected	Right ventral visual	.26	24	.20
5000	Uncorrected	Left ventral visual	-.10	23	.64
5000	Uncorrected	Right ventral visual	.07	24	.72
50	Tissue-corrected	Left ventral visual	.05	23	.81
50	Tissue-corrected	Right ventral visual	.05	24	.80
200	Tissue-corrected	Left ventral visual	.07	23	.73
200	Tissue-corrected	Right ventral visual	.22	24	.28
5000	Tissue-corrected	Left ventral visual	-.10	23	.63
5000	Tissue-corrected	Right ventral visual	.06	24	.77

Note. This table displays correlations between uncorrected and tissue-corrected GABA and fMRI distinctiveness. ROI: region of interest.